

Impact of Samarium on the Growth of Epitaxial Bismuth Ferrite Thin Films

Lutz Mühlenbein, Chandra Bhal Singh, Angelika Hähnel, Sade Campbell, Christian Hagendorf, and Akash Bhatnagar*

Doping of rhombohedral bismuth ferrite (BFO) with rare earth elements has been widely investigated as a pathway to extract ferromagnetic response from an otherwise antiferromagnetic material. However, increased level of such doping, in conjunction with the ability of BFO to accommodate large strain, has also resulted in nontrivial changes in the structure, i.e., transition to orthorhombic structure and phase separation to form vertically aligned columns. Herein, epitaxially grown and single crystalline samarium oxide (Sm_2O_3) and doped BFO films are used to investigate the structural evolution. Thin films are grown from undoped (BFO and Sm_2O_3) and doped targets, $(0.2,0.5)\text{Sm}_2\text{O}_3-(0.8,0.5)\text{BFO}$. In addition, the in-plane strain, imposed by the lattice mismatch between film and substrates, is used to demonstrate the stability of the structures formed in the doped films. Interestingly, the resultant orthorhombic structures are found to be largely independent of the underlying substrates. In-depth structural and nanoscopic measurements are conducted to investigate the structures. Ordered columnar structures, reminiscent of phase separation, are successfully obtained albeit driven by spontaneous ordering of differently oriented crystals.

1. Introduction

Thin films of bismuth ferrite (BiFeO_3 , BFO) have been intensively studied since the mid-2000s due to the intriguing ferroelectric, magnetic, and optical properties of this material.^[1] In addition, being one of the few room-temperature multiferroics, BFO is also regarded as a lead-free alternative to the widely used Pb-based piezoelectrics, but the industrial application is hindered by high leakage currents and large coercive fields.^[2] To counter this problem, and simultaneously enhance the multiferroic properties, several studies have been conducted in which the A-site of the perovskite unit cell of BFO has been partly substituted with rare earths such as samarium, with inspiration drawn from the positive impact of substitutional doping in Pb-containing ferroelectrics such as $\text{Pb}(\text{Zr,Ti})\text{O}_3$.^[3–5]

While Yuan and Or pioneered the field of Sm-doped BFO ceramics,^[6] the first synthesis of thin films of BFO-containing samarium was conducted by Driscoll et al.^[7–9] Motivated by the work on vertically aligned nanocomposites comprising of BFO and CoFe_2O_4 ,^[10] a sintered target containing BFO and Sm_2O_3 (SmO) in 1:1 molar ratio was used to grow epitaxial thin films on single-crystal SrTiO_3 substrate by pulsed laser deposition (PLD). A spontaneous phase separation into an ordered array of BFO and SmO columns was observed. It was furthermore proven that with increasing film thickness, the strain state of the film switches from lateral strain control, originating at the substrate–film interface, to vertical strain control arising from the columnar interfaces between BFO and SmO. As a consequence, the out-of-plane lattice parameter of BFO reduced from 4.000 Å in a pure BFO film to about 3.905 Å in the BFO:SmO composite film of around 50 nm film thickness. Upon comparison with the bulk value of 3.962 Å, this was interpreted as a change from in-plane compressive strain induced by the STO to out-of-plane compressive strain induced by the SmO. Although intermixing of the phases was initially not reported, it was later theorized that, although intermixing might take place during growth, the phases subsequently separate by spinodal decomposition.^[11]


However, studies conducted by Cheng et al. demonstrated that Sm^{3+} with an ionic radius of 1.24 Å, at 12-fold coordination, can substitute Bi^{3+} (1.365 Å ionic radius) at the A-site of the

L. Mühlenbein, S. Campbell, Dr. A. Bhatnagar
Zentrum für Innovationskompetenz SiLi-Nano
Martin-Luther-Universität Halle-Wittenberg
06120 Halle (Saale), Germany
E-mail: akash.bhatnagar@physik.uni-halle.de

L. Mühlenbein, Dr. A. Bhatnagar
Institute of Physics
Martin Luther Universität Halle-Wittenberg
06120 Halle (Saale), Germany

C. Bhal Singh
School of Materials Science and Technology
Indian Institute of Technology (Banaras Hindu University)
221005 Varanasi, India

Dr. A. Hähnel, Dr. C. Hagendorf
Diagnostik und Metrologie
Fraunhofer Center für Silizium-Photovoltaik
06120 Halle (Saale), Germany

 The ORCID identification number(s) for the author(s) of this article can be found under <https://doi.org/10.1002/pssb.201900625>.

© 2020 The Authors. Published by WILEY-VCH Verlag GmbH & Co. KGaA, Weinheim. This is an open access article under the terms of the Creative Commons Attribution-NonCommercial License, which permits use, distribution and reproduction in any medium, provided the original work is properly cited and is not used for commercial purposes.

DOI: 10.1002/pssb.201900625

perovskite unit cell in $\text{Bi}_{1-x}\text{Sm}_x\text{FeO}_3$ thin films synthesized by PLD^[12,13] at least up to $x = 0.3$. In addition, a phase transition from the ferroelectric rhombohedral phase with polar R3c symmetry to a paraelectric orthorhombic Pnma phase at $x = 0.14$ was observed, with a narrow transition region exhibiting antiferroelectric behavior at the phase boundary. The occurrence of such a phase transition was confirmed in another independent study^[14] and in experiments conducted on ceramic samples.^[15] Interestingly, here as well a massive reduction of the out-of-plane lattice parameter was reported with $c = 3.915 \text{ \AA}$ in a film with $x = 0.2$.

Similar observations were made in 200 nm thick films of $\text{Bi}_{0.85}\text{Sm}_{0.15}\text{MnO}_3$, where c was reduced from 3.98 \AA in a pure BiMnO_3 film to $c = 3.87 \text{ \AA}$ in the composite film, which was attributed to a reduction in Mn–O bond length and an increment in octahedral rotations.^[16,17]

Considering the diversity of results reported so far, the system of Sm-incorporated BFO can be considered as an exciting system to investigate the different realms of thin-film growth spread across conventional doping, phase separation, and change in symmetry.

In this work, we used PLD to synthesize single crystalline and epitaxial films of $x\%$ Sm-doped BiFeO_3 films with different content of Sm ($x = 0\%$, 20%, and 50%) on single-crystalline cubic STO (001) and orthorhombic TbScO_3 (TSO) (110) substrates. Well-ordered columnar structures were successfully obtained with increased levels of doping. The samples were analyzed with X-ray diffraction (XRD), transmission electron microscopy (TEM), and surface probe methods to unravel the underlying origin of the structures.

2. Results

2.1. Structural Analysis by XRD

We first focus to confirm the suitability of deposition parameters used in the current study for the ablation of BFO and SmO. This is essential since the elements involved have evidently different atomic numbers which can result in drastically different kinetic energies of the ablated species, and thus the growth rate. Time- and space-resolved optical emission spectroscopy studies in the case of LaAlO_3 and LaGaO_3 have confirmed the validity of such a scenario wherein the difference between the kinetic energies of La and Ga ions was found to be around 1.8 times.^[18] In **Figure 1**, the XRD scans acquired from pure BFO and SmO films deposited with identical deposition conditions on STO substrates are presented. The peak arising from BFO is apparently shifted to the left of the STO (002) peak, indicating an elongated out-of-plane lattice parameter c . The c_{BFO} was extracted to be around 4.06 \AA , which can be attributed to $\approx 1.5\%$ compressive strain imposed by the substrate. In the case of SmO, a sharp (004) reflection of the cubic phase is apparent. From the exact positions of the (004) peak of the cubic phase, the out-of-plane lattice parameter can be estimated to $c_{\text{SmO}} = 10.815 \text{ \AA}$. This value is slightly lower than the reported lattice parameters from the bulk cubic phase which are around 10.93 \AA .^[19] A unit cell of SmO which is rotated in-plane by 45° and positioned along [110] direction can be accommodated on STO (001), albeit under tensile strain of 1.2% .^[7,19] The reduced value of c_{SmO} supports the validity of

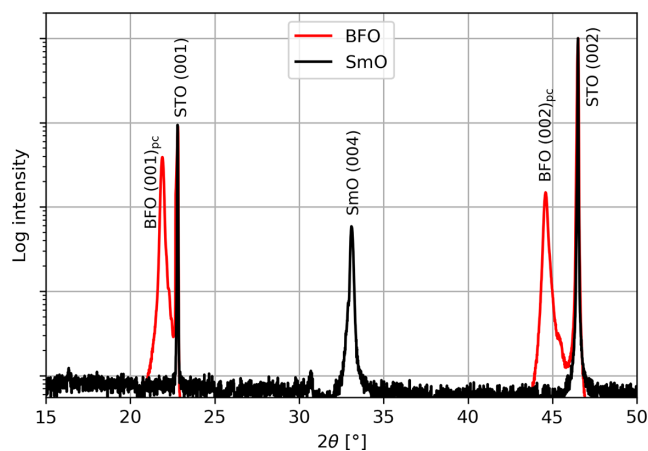


Figure 1. X-ray $\omega - 2\theta$ diffraction pattern of pure BFO and SmO thin films on STO.

such a scenario in the growth of SmO and this result is in good agreement with reports on SmO thin films on STO by Yang et al.^[19] Hence, the deposition parameters can be considered appropriate for the ablation of composite targets.

In **Figure 2a**, the X-ray $\omega - 2\theta$ diffraction pattern from thin films deposited on STO from $\text{Bi}_{1-x}\text{Sm}_x\text{FeO}_3$ targets with $x = 0$ (BFO), $x = 0.2$ (80BFSmO), and $x = 0.5$ (50BFSmO) are presented. Interestingly, separate peaks from SmO are not observed, with only the (001) and (002) reflections arising from a BFO-like perovskite phase being visible, which indicates that phase separation has not occurred. The inset presents a magnified image for the (002) reflection, where a gradual shift of the (002) reflection with increasing Sm content is evident. The extracted out-of-plane lattice parameters are plotted **Figure 3**. In particular, in the sample with the highest Sm content, 50BFSmO, the reflections from BFO and STO are almost indistinguishable, with only the presence of a slight shoulder-like feature. Identical films were also grown on TSO to observe the role of in-plane strain, if any, in the growth of the composites. In **Figure 3**, the resultant c_{BFO} have been coplotted. The in-plane strain clearly has a striking impact on the growth of pure BFO with the c_{BFO} on TSO similar to the bulk value of 3.96 \AA , and around 4.06 \AA on STO. Interestingly, the c values of the composites are largely independent of the in-plane strain as roughly identical values are extracted from the films grown on STO and TSO. A scenario wherein such independence from horizontal or in-plane strain can manifest is via the formation of vertical columns. Similar observations were made in the work from Driscoll et al. wherein the films grown from the composite target with 1:1 molar ratio of BFO and SmO resulted in BFO with highly compressed c_{BFO} nearly equaling c_{STO} , albeit with a peak arising from pure SmO also visible.^[7] Together with TEM and a thickness variation study, the existence of phase-separated columns was proven and it was claimed that the vertical strain imposed by the SmO columns prompts the massive reduction in the BFO out-of-plane lattice parameter.

Having no indication of phase separation in the XRD pattern, we cannot assume this to be the case here. On the contrary, our

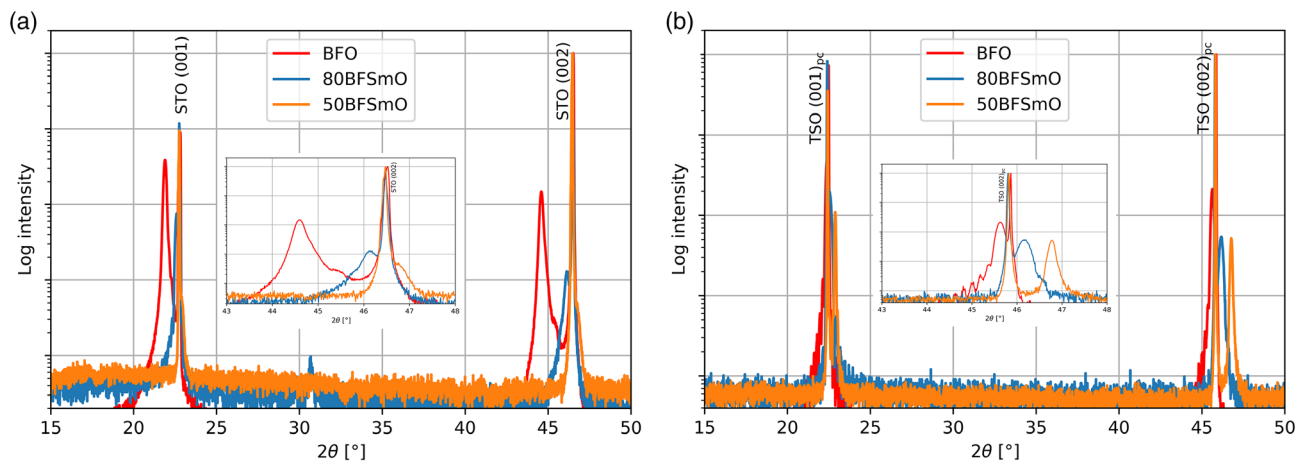


Figure 2. X-ray $\omega - 2\theta$ diffraction pattern of BF(Sm)O thin films on a) STO and b) TSO.

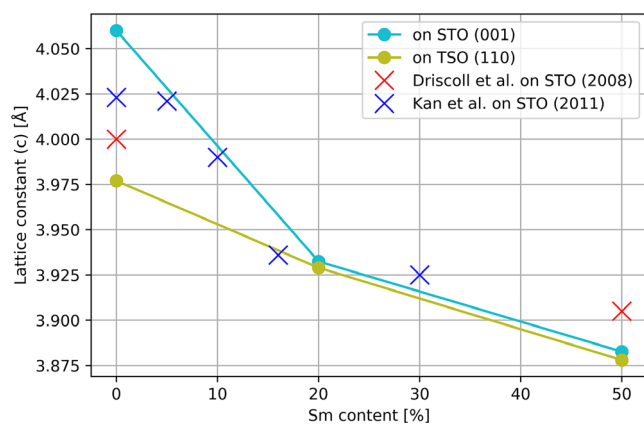


Figure 3. Out-of-plane lattice parameters of BF(Sm)O films on STO and TSO extracted from XRD. For comparison, values reported in refs. [7] and [20] from growth on STO (001) are also indicated.

results indicate that substitutional doping on the A-site as first reported by Cheng et al.^[12] can extend up to $x = 0.5$ with no phase separation taking place. Increasing Sm substitution leads to a decrease in the average ionic radius on the A-site of the perovskite unit cell, and in turn, a structural phase transition from the rhombohedral BFO-like phase to an orthorhombic phase occurs around $x = 0.14$.^[13] This seems all the more reasonable as even thin films of pure SmFeO_3 (SFO) have been grown in the orthorhombic phase on STO by PLD.^[21]

Apart from the samples grown at the parameters specified in the Experimental Section and presented here, we have also explored a broad range of the parameters available to a standard PLD system in search for phase separation, between 580 and 700 °C, 0.667 and 0.2 mbar O_2 atmosphere, and 2 and 10 Hz of laser pulse frequency, without a reliable indication of a SmO (004) peak. Also noteworthy to mention is the position of Bi_2O_3 peak, a common secondary phase in BFO,^[22] which usually appears around same value of 2θ as SmO (004). Therefore, extra caution must be exercised in the interpretation of any peak that appears within this range of 2θ .

2.2. Atomic Force Microscopy

In **Figure 4**, the surface topography of the thin films on Nb:STO as measured by atomic force microscopy (AFM) is presented. As the surface is free of precipitates and simple oxides, the respective surface roughness is governed by the grain boundaries. In agreement with existing reports,^[23] the pure BFO film on STO shows uniform grains with a lateral size parameter of about 300 nm each and root mean square (RMS) roughness of 1.687 nm. As is evident, the grain size and RMS roughness (0.441 nm) reduces significantly with increasing dopant concentration in the film with $x = 0.5$, which is also in good agreement with studies on the grain sizes in ceramic samples of Sm-doped BFO.^[15] Also, the topography and grain size in the film with $x = 0.5$ resembles very much the topography of the reported films with columnar architecture as is shown in the previous studies of Yang et al.,^[23] where the grains, however, were assumed to be nanocolumns consisting of separate BFO and SmO phases.

The resulting rectangular faceted grains in our Sm-containing samples furthermore bear striking resemblance with the surface morphology of $\text{Bi}_{0.85}\text{Sm}_{0.15}\text{MnO}_3$ thin films reported by Choi et al. where domain twinning was observed.^[16] Cheng et al. had earlier observed peak splitting in zone-axis selected-area diffraction patterns during TEM of single-phase $\text{Bi}_{0.8}\text{Sm}_{0.2}\text{FeO}_3$ thin films on STO, which they attributed to twin domains.^[12]

2.3. Transmission Electron Microscopy

To decisively determine whether a columnar nanostructure is present in our samples, we investigated cross-section focused ion beam (FIB)-lamellae of the BFSmO/STO stacks using TEM. **Figure 5a** shows TEM overviews of 80BFSmO and 50BFSmO thin films on STO substrates. The 80BFSmO film (upper pane of **Figure 5a**) seems rather homogeneously structured, whereas a clear presence of nanocolumns can be observed in the 50BFSmO film (lower pane of **Figure 5a**). In particular, the nanocolumns are perpendicular to the interface between film and substrate with diameters of 10–50 nm.

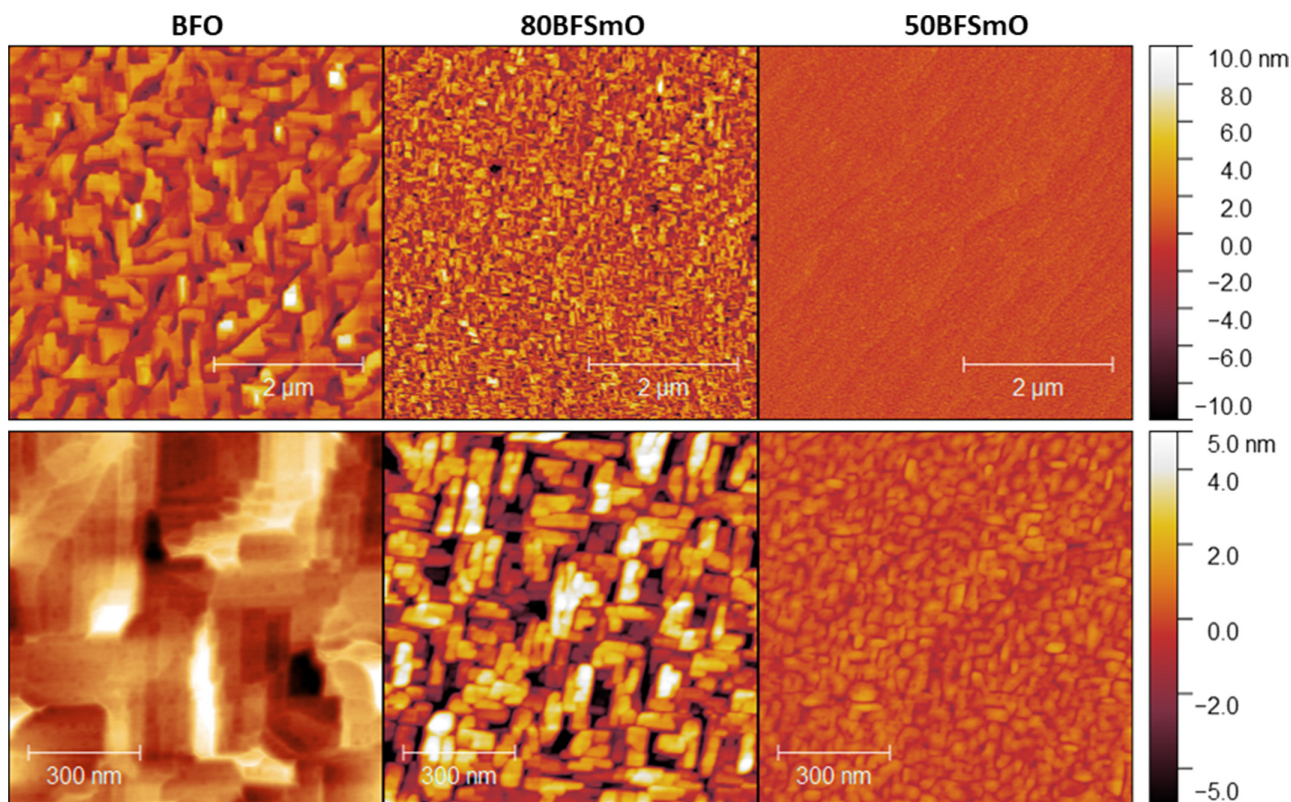


Figure 4. AFM images of BF(Sm)O thin films on STO substrate. Top row images are $5 \times 5 \mu\text{m}$, bottom row images $1 \times 1 \mu\text{m}$.

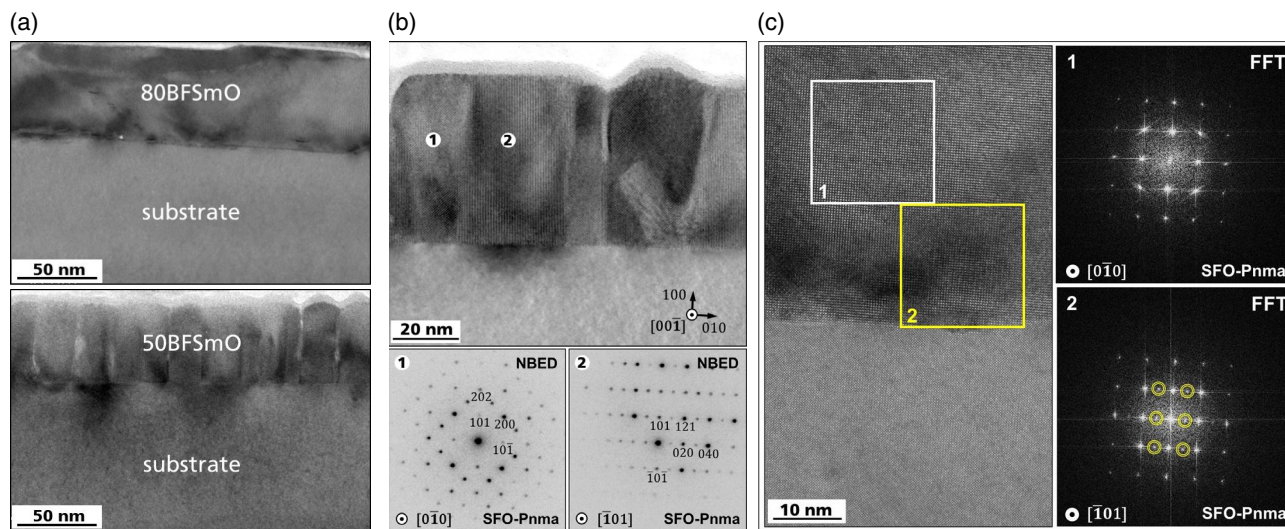


Figure 5. a) TEM results for 80BFSmO and 50BFSmO thin films on STO substrate. b) Nanobeam electron diffraction patterns from neighboring columnar regions in 50BFSmO thin film. c) HRTEM image of 80BFSmO thin film with FFT of regions 1 and 2.

To elucidate the nanochemistry of the films, energy dispersive X-ray (EDX) spectroscopy was used (not shown). However, EDX results did not show any relation between the nanocolumns and probable segregation of Bi or Sm, which implies a homogenous distribution of the two elements across the thickness of the film. Thereafter, the columns in the 50BFSmO sample were analyzed

for their respective crystallographic orientation by nanobeam electron diffraction (NBED) (Figure 5b), keeping in perspective the published data regarding the growth directions in BFSmO and SFO films on STO substrates.^[20,21] For NBED, diffraction patterns were detected by illuminating nanoregions of the sample with a nearly parallel electron-beam having a diameter of

about 3 nm. As the beam size is smaller than the diameter of the columns in the 50BFSmO film, the diffraction pattern acquired at a column includes column-specific crystallographic information. By controlled tilting in two directions, the columns were aligned in a specific relationship with the (100) plane of the substrate. The resultant NBED patterns are shown in Figure 5b. Pattern 1 and 2 were recorded from two neighboring columns (indicated in the the upper TEM image) and they clearly depict different crystallographic orientations within the columns. In particular, the diffraction patterns can be related to slightly stretched $[0\bar{1}0]$, and $[\bar{1}01]$ which are reminiscent of the observations reported in the study of SFO (space group: Pnma, $a = 0.560$ nm, $b = 0.771$ nm, $c = 0.54$ nm^[24]). Furthermore, the planes within all the investigated columns belong to (101), parallel to (100) planes of the substrate. By processing the high-resolution transmission electron microscopy (HRTEM) image in Figure 5b, the out-of-plane as well as in-plane lattice distances in both 50BFSmO-columns (indicated by 1 and 2) have been estimated to be 0.39 and 0.41 nm, respectively.

Similar values have been measured in HRTEM images of the 80BFSmO film: specifically, the lattice distances were determined to be 0.39 nm in-plane, and 0.40 nm out-of-plane. However, columnar grains do not occur in the 80BFSmO film, and rather appears to consist of a homogeneous film being locally substructured. The substructure is demonstrated in Figure 5c, which shows a HRTEM image of the film together with Fast-Fourier-Transforms (FFTs) of the film regions 1 and 2 (indicated in the TEM image). The FFT of region 2 clearly shows additional maximum peaks which indicate the local growth of $[\bar{1}01]$ -orientation similar to the one reported in SFO.

2.4. Leakage Currents

2.4.1. Capacitor Geometry

Figure 6 shows the current density (J) versus applied electric field (E) for the pure BFO and Sm-containing BFO thin films on Nb:STO. A massive reduction in leakage current, corresponding to the doping level, is evident.

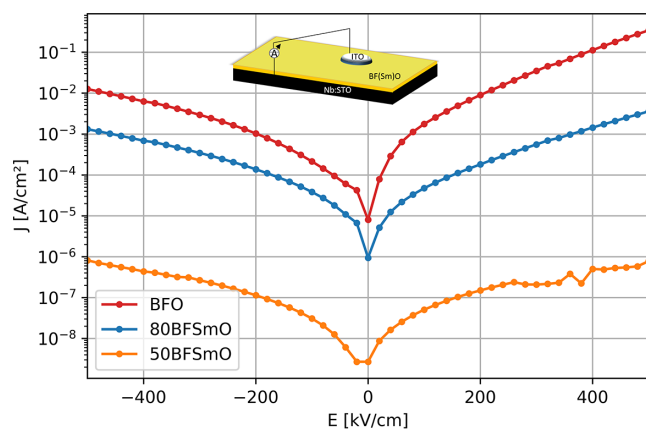


Figure 6. Leakage current density versus electric field characteristics for pure BFO and Sm-substituted BFO thin films on Nb:STO.

Interestingly, contrary results were obtained in case of ceramics, wherein much higher J have been reported in Sm-doped BFO than in pure BFO. The smaller grain size in doped-ceramics evidently translates into much large grain boundary area which was proposed to be the underlying origin for high J .^[25] However, in the case of BFSmO films with nanocolumnar architecture, results similar to the ones shown in Figure 6 were obtained,^[19] with the composite film showing J several order of magnitude lower than a pure BFO film. Similar to the morphologies presented in this work, smaller grains were also observed in the composite thin-film samples. Therefore, it was simply postulated that lowering of J , despite higher grain boundary area, can be only realized upon large reduction in oxygen vacancies. The nanocolumns apparently assist in reducing the oxygen vacancies within the BFO phase.

Although, a drastically conflicting role of largely comparable nanocolumns was demonstrated in the case of SmO–SrTiO₃ composites thin films.^[26] The interface between SmO and SrTiO₃ were measured to be much more conductive compared with the bulk of the sample and segregation of oxygen vacancies at the interface was suggested as a possible reason. The tip of conductive atomic force microscopy (CFM) was used to measure the local electrical characteristics around the interfaces. As these columns extend across the thickness of the film, the resulting macroscopic electrical measurements should result in higher values of J than previously observed,^[19] and similar to ceramics.^[25] To further investigate the origin of lower current densities in Sm-doped BFO thin films, we chose to measure the conduction properties of the samples on the nanometer scale by CFM.

2.4.2. Conductive Atomic Force Microscopy

Samples utilized for macroscopic electrical measurements were subsequently analyzed with CFM. The tip of the CFM setup was grounded during all the measurements and a bias of +4 V was applied as the tip was scanned over the surface. The samples were measured in dark conditions and under illumination. For illumination, laser of wavelength 405 nm (3.06 eV) was used which has been reported to result in a photoresponse in BFO in certain domain configurations.^[27,28] In Figure 7a–f, the topography and current scans recorded from pure BFO and x -BFSmO thin films under illumination are presented. The line profiles extracted from the scans are plotted in Figure 7g,h. Surprisingly, as evident from current scans, 50BFSmO exhibits much higher response than BFO and 80BFSmO, with grainy structure clearly visible. A rather low response is recorded from both BFO and 80BFSmO samples which does not increase above 3 pA. The difference in the respective conductivities is also apparent from the line profiles, with 50BFSmO more conductive in dark and illuminated conditions. In particular, the significant increase in the conductivity under illumination might be attributed to the lowering of bandgap that been reported in Sm-doped BFO ceramics.^[29] These results are completely contrary to the macroscopic measurements wherein BFO was found to be much more conductive and 50BFSmO the least.

A possible reason behind the discrepancy can be proposed upon analysis of the associated topographies. Although the

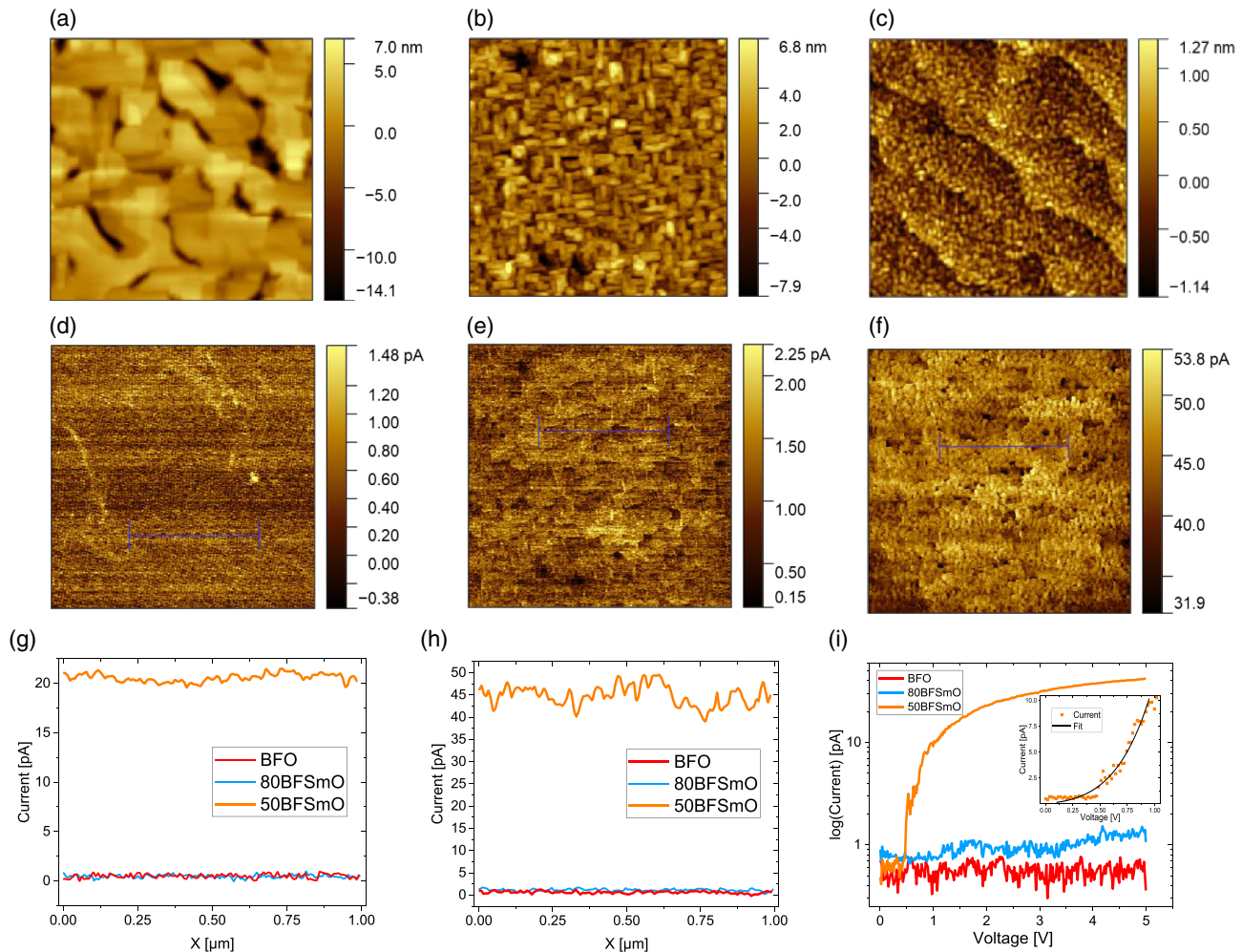


Figure 7. Conductive AFM images with $2 \times 2 \mu\text{m}$ size of BF(Sm)O thin films on Nb:STO. a,d) Present topography and current map for BFO, b,e) for 80BFSmO, c,f) for 50BFSmO thin film. Furthermore, extracted line profiles of the currents obtained in g) dark and h) illuminated conditions and local i) current–voltage characteristics are shown.

BFO surface is plagued with defects which appear as pinholes (RMS roughness of around 2.834 nm), the surface of 50BFSmO is much more smooth (RMS roughness of 0.407 nm) and homogeneous with terraces from the etched surface of the substrate still visible. Line profile across a pinhole reveals a depth of around 10 nm. However, this value is largely limited by the tip-diameter. Therefore, it can be assumed that if such defects run across the thickness of the film or partially, they will largely influence the macroscopic current response. On the contrary, a uniform current response was acquired from 50BFSmO with no drastic variations around the grain boundaries.

In conjunction, local current–voltage characteristics were measured in all the three samples and are presented in Figure 7i. In the case of pure and 80BFSmO, rather low currents were measured within the range of applied voltages. Substantial current response was recorded from 50BFSmO, which in low-voltage regimes (upto 1 V) is mostly Schottky-interface limited (inset of Figure 7i),^[30] At higher voltages, the current appears to saturate, which can be attributed to space-charge limited conduction.^[31]

3. Discussions and Conclusion

The objective of our study was to analyze the impact of samarium on the growth of BFO films. Although some results are in complete agreement with the current state of knowledge, others are distinctly contrary. The X-ray analysis clearly demonstrates a drastic reduction in the value of c_{BFO} as the content of Sm is increased, to the level it reaches 3.90 Å and matches c_{STO} . Growth on TSO substrates results in identical values of c_{BFO} as obtained in the case of STO, implying minimalistic role of in-plane strain. TEM investigations allowed us to unravel this mystery and suggest that the BFSmO films comprise of orthorhombic crystals that are aligned along [100] and [110], which apparently results in lowering of macroscopic c_{BFO} value. This assessment is in full agreement with other reports wherein Sm content of upto 30% has been studied and in the case of pure SmFeO₃ films.^[12,21] However, in our study, such an assessment is valid even upto 50% Sm, wherein the crystals were observed to be ordered in a dense columnar arrangement with a rather sharp interface in-between.

Curiously, a phase separation has been often reported in 50% Sm-BFO^[7–9] which coincidentally also proceeds via the formation of alternating nanocolumns, resembling the ordering observed in this work. Another point of resemblance is the c_{BFO} which was found to be largely reduced due to the vertical strain imposed by the lattice-mismatched SmO phase. The resemblance further continues to macroscopic electrical characteristics, which qualitatively were found to be alike.^[9] But, with our nanoscopic measurements, we were able to conclude that although the pure BFO exhibit larger crystal size (implying lower grain boundary area) than 50BFSmO, the densely packed crystals in 50BFSmO ensure that bulk of the sample determines the electrical response, unlike BFO wherein the pinhole-like feature can massively dominate the electrical response. Therefore, it can be proposed that electrical response in widely reported phase-separated SmO-BFO is not determined by the in-between nanocolumns, as previously perceived, but by the orthorhombic BFSmO itself. An in-depth analysis to rule out the scenario of substitutional doping is a prerequisite, which has been inadvertently not sufficiently addressed in the work pertaining to phase separation. In addition, the 50BFSmO was found to be around two orders of magnitude more conductive than pure BFO, in contrast to previous reports.^[9]

Nevertheless, the question about the absence of the phase-separated columns in our study still remains. Considering we chose very similar deposition and cooling parameters as in the literature cited earlier and also explored a wide range of parameters available to a standard PLD system, it remains unclear what exactly triggers phase separation during PLD growth in a combination of compounds that—according to multiple preceding work and the results presented here—exhibit intermiscibility. Attention here could be brought to the ablation process and characteristics of the target. One could imagine a situation in which differences in the preparation of the target concerning the density and present phases influence the individual kinetic energies of ionic species in the plasma plume in a way that phase separation can take place in one case but not in the other. This however is only relevant if the columnar growth takes place during the actual deposition itself, with the columns originating at the film–substrate interface due to different interfacial energies of the separate phases—such as, for example, in the BFO-CoFe₂O₄ system.^[32] If, as has been retroactively theorized,^[33] the separation is due to spinodal decomposition, more attention should in turn be brought to the cooling process. The observation of phase-separated columns only in the top half of an BiMnO₃-SmO film^[34] might support this scenario. However, a cohesive study regarding the influence of cooling parameters is still missing.

The earlier discussion clearly highlights the intricacies involved in the system of rare-earth-doped BFO system. In our systematic investigation, we have explicitly unraveled a new scenario wherein 50%-doped BFO results in columnar structures, that is not driven by phase separation but by spontaneous ordering of crystals which are differently oriented, and uniformly doped. The results are also of relevance to the study of magnetic response in rare-earth-element-doped BFO wherein high concentration and uniform distribution of dopant is desired rather than phase separation.

4. Experimental Section

Single-crystals of STO (001), Nb-doped STO (001) (Nb:STO), and TSO (110) from CrysTec GmbH were used as substrates. The STO and Nb:STO substrates were prepared with an HF-based etching process and subsequent annealing step to ensure TiO₂-termination and atomically flat surface,^[35] whereas the TbScO₃ substrates were annealed at 1000° for 2 h without etch treatment.

PLD with an KrF excimer laser was used to synthesize the thin films by ablating from stoichiometric targets of Bi_{1-x}Sm_xFeO₃ with $x = 0$, $x = 0.2$ and $x = 0.5$, as well as a pure Sm₂O₃. If not specified otherwise, samples were deposited at a substrate temperature of 625° in 0.133 mbar O₂ atmosphere with a laser fluence and repetition rate of about 1 J cm⁻² and 2 Hz, respectively. Thereafter, the samples were cooled at a controlled rate of 20 K min⁻¹ in 200 mbar of oxygen environment. Thickness of around 50 nm was obtained in all the samples.

The topographies of the samples were analyzed with Park NX10 AFM. The crystal structure of the samples was analyzed with a Bruker D8 Discover X-ray diffractometer. TEM was used for an in-depth investigation on a nanometer scale. Electron-transparent lamellae were prepared in cross-section orientation by FIB using a dual-FIB/SEM FEI Versa3D (FEI Thermo Fisher Scientific Inc.). The lamellae were subjected to structural and chemical analyses using both TEM/STEM FEI TecnaiG2 F20 and TEM/STEM FEI Titan3G2 60-300 being dedicated to EDX spectroscopy by a SuperX Si-drift EDX-detector system (FEI Thermo Fisher Scientific Inc.).

Macroscopic current–voltage characteristics were measured with transparent top electrodes of indium tin oxide (ITO) that were deposited on the thin films, with Nb:STO serving as the bottom electrode. Circular electrodes of diameter 100 μm were patterned with photolithography. ITO was deposited with PLD at room temperature in 0.08 mbar O₂ atmosphere from a stoichiometric target.

For conductive AFM measurements, NSC15 platinum-coated tips from Mikromasch were used. The current acquired from the tip was fed into a low-noise current amplifier from Femto. The output from the amplifier was directed into the AFM controller to record the images of current scans.

Acknowledgements

The authors thank Prof. Kathrin Dörr and Dr. Diana Rata for the X-ray measurements, Marian Lisca for the technical support, Dr. Bodo Fuhrmann, and Dipl.-Phys. Sven Schlenker for their support with the facilities at the Interdisziplinäre Zentrum für Materialwissenschaften (IZM). Financial support from Deutsche Forschungsgemeinschaft (DFG) via Sonderforschungsbereiche (SFB) 762 (project A12), Bundesministerium für Bildung und Forschung (BMBF) Project No. 03Z22HN12, and Europäischer Fonds für regionale Entwicklung (EFRE) Sachsen-Anhalt is gratefully acknowledged.

Conflict of Interest

The authors declare no conflict of interest.

Keywords

bismuth ferrite, composite thin films, pulsed laser deposition, samarium oxide, vertically aligned nanocomposites

Received: September 30, 2019

Revised: February 13, 2020

Published online: February 28, 2020

[1] D. Sando, A. Barthélémy, M. Bibes, *J. Phys.: Condens. Matter* **2014**, *26*, 473201.

- [2] C. H. Yang, D. Kan, I. Takeuchi, V. Nagarajan, J. Seidel, *Phys. Chem. Chem. Phys.* **2012**, *14*, 15953.
- [3] R. E. Eitel, C. A. Randall, T. R. Shrout, P. W. Rehrig, W. Hackenberger, S. E. Park, *Jpn. J. Appl. Phys.* **2001**, *40*, 5999.
- [4] B. Jaffe, *Piezoelectric Ceramics*, 1st ed., Elsevier Academic Press, London **1971**.
- [5] B. Jaffe, R. S. Roth, S. Marzullo, *J. Res. Natl. Bur. Stand.* **1955**, *55*, 239.
- [6] G. L. Yuan, S. W. Or, *J. Appl. Phys.* **2006**, *100*, 024109.
- [7] J. L. MacManus-Driscoll, P. Zerrer, P. Zerrer, H. Wang, H. Wang, H. Yang, H. Yang, J. Yoon, J. Yoon, A. Fouchet, A. Fouchet, R. Yu, R. Yu, M. G. Blamire, M. G. Blamire, Q. Jia, Q. Jia, *Nat. Mater.* **2008**, *7*, 314.
- [8] Z. Bi, J. H. Lee, H. Yang, Q. Jia, J. L. MacManus-Driscoll, H. Wang, *J. Appl. Phys.* **2009**, *106*, 094309.
- [9] H. Yang, H. Wang, J. Yoon, Y. Wang, M. Jain, D. M. Feldmann, P. C. Dowden, J. L. MacManus-Driscoll, Q. Jia, *Adv. Mater.* **2009**, *21*, 3794.
- [10] H. Zheng, F. Straub, Q. Zhan, P. L. Yang, W. K. Hsieh, F. Zavaliche, Y. H. Chu, U. Dahmen, R. Ramesh, *Adv. Mater.* **2006**, *18*, 2747.
- [11] W. Zhang, R. Ramesh, J. L. MacManus-Driscoll, H. Wang, *MRS Bull.* **2015**, *40*, 736.
- [12] C. J. Cheng, D. Kan, S. H. Lim, W. R. McKenzie, P. R. Munroe, L. G. Salamanca-Riba, R. L. Withers, I. Takeuchi, V. Nagarajan, *Phys. Rev. B* **2009**, *80*, 014109.
- [13] D. Kan, L. Pálová, V. Anbusathaiah, C. J. Cheng, S. Fujino, V. Nagarajan, K. M. Rabe, I. Takeuchi, *Adv. Funct. Mater.* **2010**, *20*, 1108.
- [14] N. H. Hong, N. Thu Huong, T. Y. Kim, S. Goumri-Said, M. B. Kanoun, *J. Phys. Chem. C* **2015**, *119*, 14351.
- [15] E. Gil-gonzález, A. Perejón, P. E. Sánchez-Jiménez, M. A. Hayward, J. M. Criado, M. J. Sayagués, L. A. Pérez-Maqueda, *J. Alloys Compd.* **2017**, *711*, 541.
- [16] E. M. Choi, A. Kursumovic, O. J. Lee, J. E. Kleibecker, A. Chen, W. Zhang, H. Wang, J. L. Macmanus-Driscoll, *ACS Appl. Mater. Interfaces* **2014**, *6*, 14836.
- [17] E. M. Choi, J. E. Kleibecker, J. L. MacManus-Driscoll, *Sci. Rep.* **2017**, *7*, 43799.
- [18] S. Amoruso, C. Aruta, P. Aurino, R. Bruzzese, X. Wang, F. M. Granozio, U. S. di Uccio, *Appl. Surf. Sci.* **2012**, *258*, 9116.
- [19] H. Yang, H. Wang, H. M. Luo, D. M. Feldmann, P. C. Dowden, R. F. DePaula, Q. X. Jia, *Appl. Phys. Lett.* **2008**, *92*, 2.
- [20] D. Kan, C. J. Cheng, V. Nagarajan, I. Takeuchi, *J. Appl. Phys.* **2011**, *110*, 014106.
- [21] Z. Cheng, F. Hong, Y. Wang, K. Ozawa, H. Fujii, H. Kimura, Y. Du, X. Wang, S. Dou, *ACS Appl. Mater. Interfaces* **2014**, *6*, 7356.
- [22] H. Béa, M. Bibes, A. Barthélémy, K. Bouzehouane, E. Jacquet, A. Khodan, J. P. Contour, S. Fusil, F. Wyczisk, A. Forget, D. Lebeugle, D. Colson, M. Viret, *Appl. Phys. Lett.* **2005**, *87*, 072508.
- [23] H. Yang, H. Wang, G. F. Zou, M. Jain, N. A. Suvorova, D. M. Feldmann, P. C. Dowden, R. F. DePaula, J. L. MacManus-Driscoll, A. J. Taylor, Q. X. Jia, *Appl. Phys. Lett.* **2008**, *93*, 142904.
- [24] E. N. Maslen, V. A. Streltsov, N. Ishizawa, *Acta Crystallogr., Sect. B* **1996**, *52*, 406.
- [25] K. S. Nalwa, A. Garg, *J. Appl. Phys.* **2008**, *103*, 044101.
- [26] S. Lee, A. Sangle, P. Lu, A. Chen, W. Zhang, J. S. Lee, H. Wang, Q. Jia, J. L. MacManus-Driscoll, *Adv. Mater.* **2014**, *26*, 6284.
- [27] A. Bhatnagar, A. Roy Chaudhuri, Y. Heon Kim, D. Hesse, M. Alexe, *Nat. Commun.* **2013**, *4*, 2835.
- [28] D. S. Knoche, Y. Yun, N. Ramakrishnegowda, L. Mühlenbein, X. Li, A. Bhatnagar, *Sci. Rep.* **2019**, *9*, 13979.
- [29] C. S. Tu, C. S. Chen, P. Y. Chen, H. H. Wei, V. H. Schmidt, C. Y. Lin, J. Anthoniappen, J. M. Lee, *J. Eur. Ceram. Soc.* **2016**, *36*, 1149.
- [30] J. Seidel, P. Maksymovych, Y. Batra, A. Katan, S. Y. Yang, Q. He, A. P. Baddorf, S. V. Kalinin, C. H. Yang, J. C. Yang, Y. H. Chu, E. K. H. Salje, H. Wormeester, M. Salmeron, R. Ramesh, *Phys. Rev. Lett.* **2010**, *105*.
- [31] S. Farokhipoor, B. Noheda, *Phys. Rev. Lett.* **2011**, *107*, 127601.
- [32] H. Zheng, Q. Zhan, F. Zavaliche, M. Sherburne, F. Straub, M. P. Cruz, L. Q. Chen, U. Dahmen, R. Ramesh, *Nano Lett.* **2006**, *6*, 1401.
- [33] J. L. Macmanus-Driscoll, *Adv. Funct. Mater.* **2010**, *20*, 2035.
- [34] A. Chen, Z. Bi, Q. Jia, J. L. MacManus-Driscoll, H. Wang, *Acta Mater.* **2013**, *61*, 2783.
- [35] G. Koster, G. Rijnders, D. H. Blank, H. Rogalla, *Physica C* **2000**, *339*, 215.